Conf-9105231--1

CONF-9105231--1

DE91 015304

THE ELECTROMAGNETIC SCENARIO FOR HIGGS PRODUCTION IN LARGE COLLIDERS

C. Bottcher and M. R. Strayer

Center for Computationally Intensive Physics

Physics Division, Oak Ridge National Laboratory

Oak Ridge, TN 37831

ABSTRACT

We outline the formalism required to calculate coherent pair production from electromagnetic fields. Applications are made to the production of the Higgs boson at large colliders, with particular attention to the problem of discriminating against backgrounds. Electromagnetic production does indeed appear to be a competitive probe of the symmetry-breaking sector.

MASTER

DISCLAIMER

This report was prepared as an account of work sponsored by an agency of the United States Government. Neither the United States Government nor any agency thereof, nor any of their employees, makes any warranty, express or implied, or assumes any legal liability or responsibility for the accuracy, completeness, or usefulness of any information, apparatus, product, or process disclosed, or represents that its use would not infringe privately owned rights. Reference herein to any specific commercial product, process, or service by trade name, trademark, manufacturer, or otherwise does not necessarily constitute or imply its endorsement, recommendation, or favoring by the United States Government or any agency thereof. The views and opinions of authors expressed herein do not necessarily state or reflect those of the United States Government or any agency thereof.

"The submitted manuscript has been authored by a contractor of the U.S. Government under contract No. DE-AC05-84OR21400. Accordingly, the U.S. Government retains a nonexclusive, royalty-free license to publish or reproduce the published form of this contribution, or allow others to do so, for U.S. Government purposes."

DISTRIBUTION OF THIS DOCUMENT IS UNLIMITED

1. INTRODUCTION

During the collision of heavy ions at relativistic velocities, large transient electromagnetic fields are formed in a space-time region near the collision [1,2]. These fields are sufficiently intense to produce large numbers of electron, muon and tauon pairs, [3,4] as well as other more massive particles [5,6]. It is also possible to produce the Higgs [6,7] via its coupling to two photons through charged fermion and boson loops. The central issue in searching for the yet-undiscovered Higgs boson is how to separate the decay products of the signal from background events. Electromagnetic production may have a competitive advantage insofar as the transverse components of the fields just outside the colliding nuclei are sufficiently large that triggering on peripheral events provides a simple way of removing the backgrounds from hadronic decays [7].

The plan of this paper is as follows. In Section 2 we outline the formalism needed to describe coherent pair production from electromagnetic fields. To illustrate the general features of the process, particularly the role of nuclear form factors, we present results for electron and heavier lepton pairs in Section 3. In Sections 4 and 5 we proceed to calculations on electroweak boson and Higgs production, with attention to the question of central event suppression, and backgrounds; incoherent production mechanisms are also briefly considered.

We conclude that the electromagnetic scenario has distinct competitive advantages as a clean probe of the electroweak and symmetry-breaking sectors.

2. PAIR PRODUCTION BY ELECTROMAGNETIC FIELDS

Collisions of bare heavy ions (for present purposes, those heavier than $Z = 70$) may, in principle, produce pairs of any charged particle out of the vacuum,

$$A_Z^{Z+} + A_Z^{Z+} \longrightarrow A_Z^{Z+} + A_Z^{Z+} + \chi^+ + \chi^- \,, \tag{1}$$

where χ may stand for $e, \mu, \tau, W \ldots$; yet other particles may be formed by merging two photons (e.g. the π^0) or by forming a triangle diagram (e.g. the Higgs ϕ^0). In a collider geometry each ion has a Lorentz γ given by

$$\gamma = \frac{1}{\sqrt{1-\beta^2}} \simeq (E/A)\ \mathrm{GeV}. \tag{2}$$

The equivalent fixed target energy is $\gamma_{\mathrm{FT}} = 2\gamma^2 - 1$, and it is this number which determines the tranverse field in the frame of one nucleus, which is, in turn, responsible for pair production. Fig. 1 illustrates schematically the

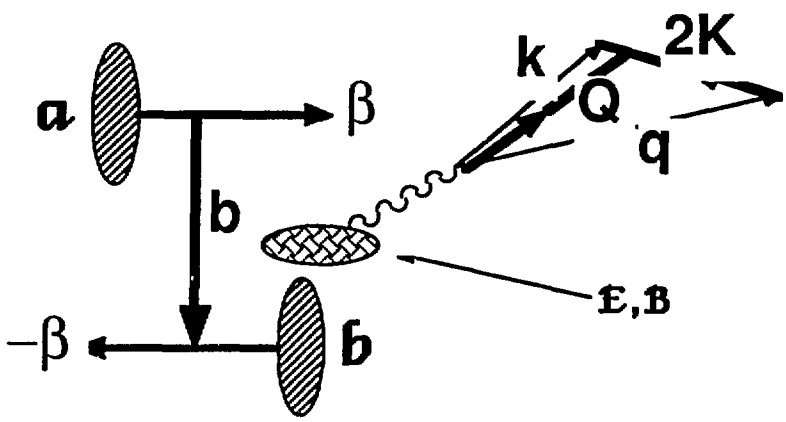

Fig. 1. Pair production in a relativistic heavy ion collision.

production of a pair from the electromagetic fields of colliding ions,

$$\mathcal{E}, \mathcal{B} \sim \frac{Z\gamma_{\mathrm{FT}}}{b^2}. \tag{3}$$

The electric field peaks at the distance of closest approach where it is predominantly transverse. The momenta $\vec{k}_1, \vec{k}_2$ of a light pair (electrons or muons, say) are predominantly in the beam direction, but very heavy pairs (such as W bosons) acquire little momentum in this direction and are emitted almost perpendicularly. To provide a frame of reference, Table 1 lists γ and γ_{FT} in round numbers for present and forseeable heavy-ion colliders. Some fixed target machines (AGS and SPS) are listed as though they were colliders. No plans exist at the time of writing to inject heavy ions into the largest machines, SSC and ELOISATRON [7].

Table 1

Energies of Heavy-Ion Colliders.

Facility	γ	γ_{FT}
AGS	3	17
SPS	10	200
RHIC	100	2×10^4
LHC	2000	8×10^6
SSC	8000	13×10^7
ELOISATRON	4×10^4	3×10^9

The central physics question raised by the heavy ion–electromagnetic field scenario for producing new particles is: granted the field strengths are very impressive, what is the advantage over proton collisions in which the energy and charge currents are much higher? The response, in two parts, is as follows:

- For large enough energies, the protons bound in the nuclei act coherently, so

that the effective current is amplified by Z^2 rather than Z, or a factor of Z^4 in the total cross section.

- A substantial part of the electromagnetic production is peripheral, coming from collisions associated with small hadronic backgrounds. This contrasts with purely hadronic mechanisms like gluon fusion which are inherently short range and require central collisions.

Both statements must, of course, be investigated by detailed calculations. However the issue of coherence can be discussed in fairly simple terms. To produce a pair of total mass $2M$ coherently, it is necessary that the recoil in the frame of each nucleus be less than 0.025GeV, the maximum excitation possible without fragmentation,

$$\frac{2Mc^2}{2\gamma} \lesssim 0.025\text{GeV}. \tag{4}$$

Thus to produce W pairs, $\gamma \gtrsim 3000$. The condition (4) is equivalent to the statement that the size of the Lorentz-contracted nuclear charge distribution must be less than a Compton wavelength,

$$\frac{R_n}{\gamma} \lesssim \lambda_c, \tag{5}$$

where the nuclear radius $R_n \sim 8\,\text{fm}$.

We shall introduce the theoretical methods used by outlining the calculation of lepton pair production. In the quantum field theory treatment we start from the interaction Hamiltonian for charged leptons and photons in a minimal coupling model. In terms of the normally ordered lepton fields $\psi(x)$, and the electromagnetic currents and fields, respectively $J_\mu(x)$ and $A_\mu(x)$,

$$\mathcal{H}_{\rm int}(x) = e : \bar{\psi}(x)\gamma^\mu\psi(x)\, A_\mu(x) : + e : J^\mu(x) A_\mu(x) : , \tag{6}$$

For spin-zero nuclei we assume that the current is specified by its matrix elements

$$< \vec{p}_a^{\,'} | J^\mu(x) | \vec{p}_a >= (p_a^\mu + p_a^{'\mu}) Z_a F(-q_a^2) \exp(-iq_a \cdot x) \tag{7}$$

for nucleus a, with a similar expression for nucleus b. The momentum transfer is given in terms of the initial and final momentum of the nucleus, $q_a = p_a - p_a^{'}$, as

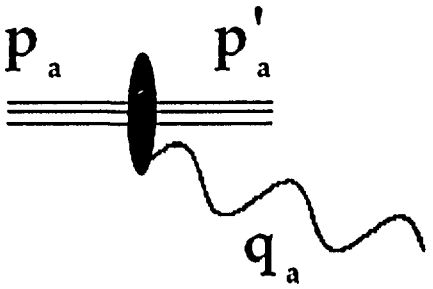

Fig. 2. Momenta at heavy ion–photon vertex.

shown in Fig. 2. Successive terms in the S-matrix are given by the Feynman rules. The leading diagrams which describe the production of a pair of leptons are given in Fig. 3. The cross section can be written as

$$\sigma_{ab\to\ell\bar{\ell}} = \frac{1}{2\beta}\frac{1}{2\omega_a 2\omega_b}\int \frac{d^3p_a^{'} d^3p_b^{'}}{(2\pi)^6 2\omega_a^{'} 2\omega_b^{'}} \int \frac{d^3k_1 d^3k_2}{(2\pi)^6 2E_1 2E_2}(2\pi)^4$$
$$\times\, \delta^4(p_a + p_b - k_1 - k_2 - p_a^{'} - p_b^{'}) \sum_{s_1,s_2} |\mathcal{M}|^2 , \tag{8}$$

where the invariant matrix element is given by

$$\mathcal{M} = -ie^4 (p_a + p_a^{'})_\mu Z_a \frac{F_a(-q_a^2)}{q_a^2} (p_b + p_b^{'})_\nu Z_b \frac{F_b(-q_b^2)}{q_b^2}$$
$$\times\, \bar{u}(\vec{k}_1, s_1)\{\gamma^\mu \frac{1}{\not{k} - m}\gamma^\nu + \gamma^\nu \frac{1}{\not{k}' - m}\gamma^\mu\} v(\vec{k}_2, s_2) . \tag{9}$$

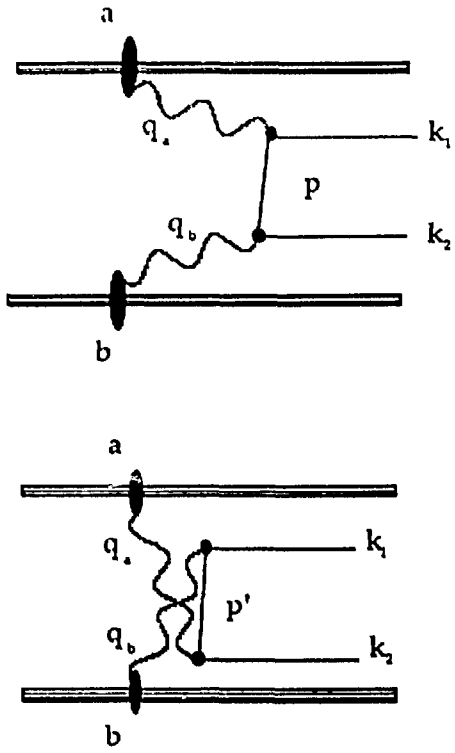

Fig. 3. Feynman diagrams for two-photon lepton pair production.

In these expressions, ω_i and ω_i' denote the total energies of the ingoing and outgoing nuclei.

The above expressions correspond to the lowest-order (two-photon) processes which can create pairs. To recover the classical field result, we assume that the momentum carried by the virtual photon is small in relation to the momentum carried by the nucleus. In this case

$$\omega \simeq \omega' , \quad p_\mu + p'_\mu = 2p_\mu + q_\mu = 2\omega u_\mu , \tag{10}$$

where the four velocities u are defined for a or b as,

$$u^\mu_{a,b} = (1, 0, 0, \pm\beta) . \tag{11}$$

It can be proved formally from gauge invariance (and numerically confirmed) that the q_μ term in the current does not contribute. Using these approximations we have

$$\sigma_{ab\to\ell\bar{\ell}} = \frac{Z_a^2 Z_b^2 (4\pi\alpha)^4}{2\beta} \int \frac{d^3k_1 d^3k_2 d^3q_a}{(2\pi)^8 2E_1 2E_2} (2\pi)\delta(q_a^0 + q_b^0 - k_1^0 - k_2^0) f_a^2(q_a^2) f_b^2(q_b^2)$$
$$\times \sum_{s_1,s_2} |\bar{u}(\vec{k}_1, s_1)\{\not{\mu}_a \frac{1}{\not{k} - m} \not{\mu}_b + \not{\mu}_b \frac{1}{\not{k}' - m} \not{\mu}_a\} v(\vec{k}_2, s_2)|^2 \,. \tag{12}$$

With a modest amount of analysis, the momenta of the virtual photons are found to be

$$q_a^0 - \beta q_a^3 = \nu_a/\gamma \,, \quad q_b^0 + \beta q_b^3 = \nu_b/\gamma \,, \tag{13}$$

where ν is the energy of the photon in the rest frame of each nucleus. The initial and final nuclear states must be "on-shell", so that ν is given in terms of the mass of the nucleus M, and the square of the photon momentum q^2, by $\nu = q^2/2M$. Since ν is negative definite in the nuclear rest frame, the virtual photons are always "space-like". The magnitude of the square of the momentum transfer is governed by the form factor of the nucleus. For values of q greater than the inverse nuclear size, the form factor becomes very small. Thus, if R denotes the nuclear radius, $\|q\| \leq 1/R$, which is about 25 MeV for heavy nuclei. This implies that for heavy-ion beams at RHIC or machines of higher energy, $\nu/\gamma \lesssim 10^{-6} \times \|q\|$. Under these conditions, the right side of (13) can be ignored and (12) simplifies to,

$$\sigma_{ab\to\ell\bar{\ell}} = \frac{Z_a^2 Z_b^2 (4\pi\alpha)^4}{4\beta^2} \int \frac{d^3k_1 d^3k_2 d^2q_{a\perp}}{(2\pi)^8 2E_1 2E_2} f_a^2(q_a^2) f_b^2(q_b^2)$$
$$\times \sum_{s_1,s_2} |\bar{u}(\vec{k}_1, s_1)\{\not{\mu}_a \frac{1}{\not{k} - m} \not{\mu}_b + \not{\mu}_b \frac{1}{\not{k}' - m} \not{\mu}_a\} v(\vec{k}_2, s_2)|^2 \,. \tag{14}$$

This is identical with the classical field approximation [3].

In summary, the classical field approximation is realized whenever the energy momentum of the virtual photons is small compared with the nuclear momentum, as is usually the case for large γ. Factorizing the product of flux factors and cross sections, as is done in the equivalent photon prescription, is a further approximation which we do not make in the classical field approach. Rather, we integrate the cross section directly by Monte Carlo methods [8].

In practice, we use space-like form factors from empirical charge distributions, ρ, which are fitted to low-energy electron scattering data [9]. The bulk properties of the nuclear charge density, the magnitude of the central density, the surface thickness, and the radius are often given in terms of a Fermi function,

$$\rho(r) = \frac{\rho_0}{1 + \exp[(r - R)/a)]} , \tag{15}$$

where for heavy nuclei, $R = 1.10A^{1/3}$ fm, A being the mass number of the nucleus. The surface thickness parameter is $a = 0.55$ fm and the constant ρ_0 is fixed by the normalization condition, $\int d^3r \ \rho(r) = 1$. For this parametrization of the charge density, $F(-q^2)$ may be expressed analytically [6]. The variation of the form factor squared with momentum transfer $\sqrt{-q^2}$ is shown in Fig. 4. The filled circle indicates the scale appropriate to muon production: electrons are sensitive to lower momenta and heavy bosons to much higher momenta.

One of the important differences between most equivalent photon methods and the present work is the treatment of the nuclear surface. These methods generally

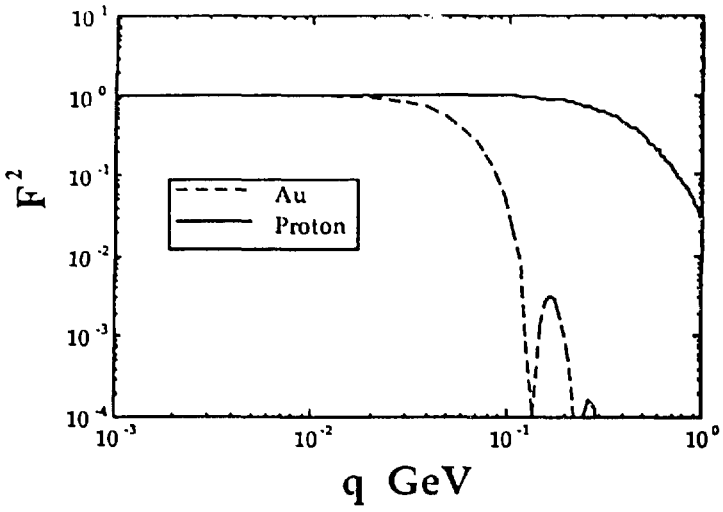

Fig. 4. Nucleon and nuclear form factors *vs* momentum transfer.

use a sharp cutoff model in which momentum integrals are limited by $1/R$. For the very peripheral collisions this ignores surface effects.

3. SOME RESULTS ON LEPTON PRODUCTION

To provide a reference point, we show in Fig. 5 the variation of the two- photon cross section for electron-positron production by unit point charges calculated in various approximations [3,4]. The Monte-Carlo, or Racah, results are practically identical and may be regarded as exact. This result scales with mass and charge as Z^4/M^2 for any point charges and provides an upper bound for any calculation including a form factor. The point to take away is that the two-photon cross sections for heavy ions start from a large baseline: however they may be reduced by form factors. For Au+Au at RHIC, the total electron σ = 33Kb.

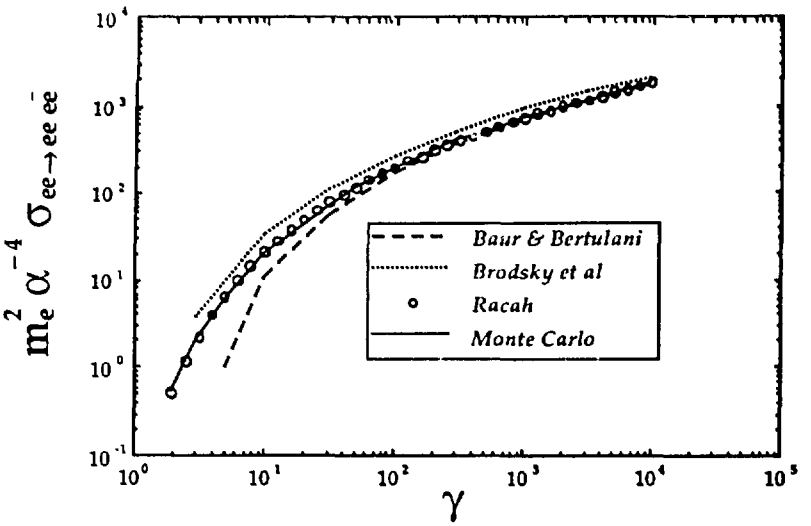

Fig. 5. Total electron pair production *vs* energy.

As a consequence, the tails at energies of a few GeV provide substantial backgrounds of many mb, which must be accounted for in detector design. The tails are sensitive to form factors, as illustrated by Fig. 6 which shows the rapidity distribution for three different models. Clearly, the correct choice of form factor is important. An overview of muon and tauon production as a function of energy is given in Fig. 7. The qualitative behavior of such cross sections can be explained as follows. Consider the simple schematic model of a collision in which the nuclei each emit a virtual photon, q'_a, q'_b, in the rest frame of each respective nucleus, $q'_a = -q'_b = (0,0,0,q)$. The form factors $F_a(-q'^2_a)^2$ and $F_b(-q'^2_b)^2$ represent the probability that each nucleus will emit the corresponding photon and remain in their ground state. The form factors control the magnitude of the emission, which is strongly suppressed whenever the momentum transfer is much larger than the

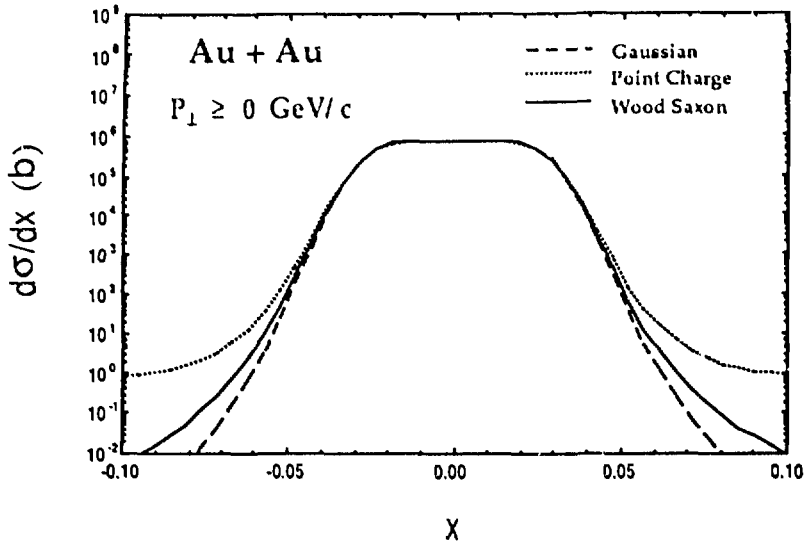

Fig. 6. Effect of the form factor on electron pair production.

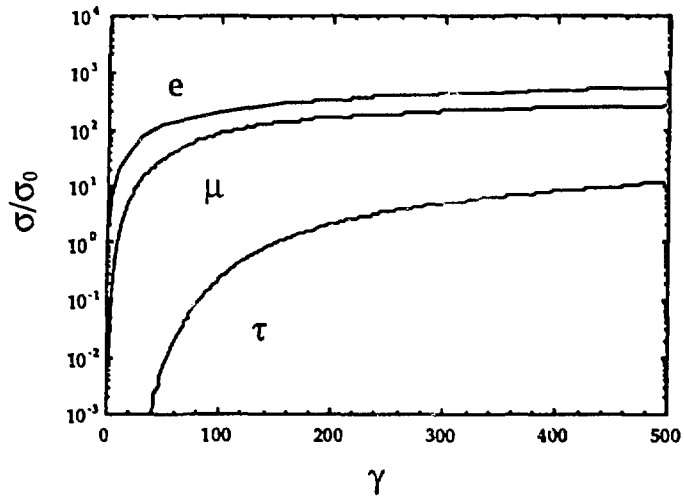

Fig. 7. Total muon and tauon pair production *vs* energy.

inverse nuclear size, $-q'^2 \gg 1/R^2$. Referring to the kinematical relations which determine q_a and q_b, we recover the criteria of (4) or (5). Table 2 shows the momentum threshold, $q_T = 2M/\gamma$, and the corresponding suppression due to the form factor for several systems of pairs from Au collisions at RHIC.

Table 2

Suppression of the coherent cross section due to the nuclear electromagnetic form factor for Au + Au collisions at RHIC ($\gamma \sim 100$).

	m (GeV)	$m\gamma$ (GeV)	F^4
e^+e^-	5.11×10^{-4}	5×10^{-6}	~ 1
$\mu^+\mu^-$	0.106	10^{-3}	~ 1
$\tau^+\tau^-$	1.784	2×10^{-2}	0.5
$b\bar{b}$	5.0	5×10^{-2}	10^{-2}
W^+W^-	81	0.8	10^{-16}

At this energy, coherent production of electron pairs is hardly affected by the form factor, and muon and tauon production only moderately. For heavier mass pairs, b-quarks, and W boson pairs, the production is greatly suppressed by the form factor unless one goes to much higher energies. As the beam energy decreases, the threshold momentum increases to large values of Q^2, and the pair production is sensitive to the high momentum part of the form factor. In this kinematic régime the cross section exhibits a very strong dependence on the collision energy. When the threshold momentum corresponds to small values of Q^2, the pair cross section dependence on beam energy saturates, going over to its logarithmic asymptotic form. In the asymptotic régime the production is no longer suppressed, and indeed the magnitude of the cross section is not sensitive to details of the form factor. It is in this régime that the full Z^4 coherence is recovered, though suppressed by a factor of about $1/A$ due to the form factor.

Since muon production is only reduced by a factor of three below the point charge result at asymptotic energies, electromagnetic muons also constitute significant backgrounds. It is instructive to compare a typical cross section with that for the well-known Drell-Yan mechanism. Fig. 8 shows that for Au collisions at RHIC,

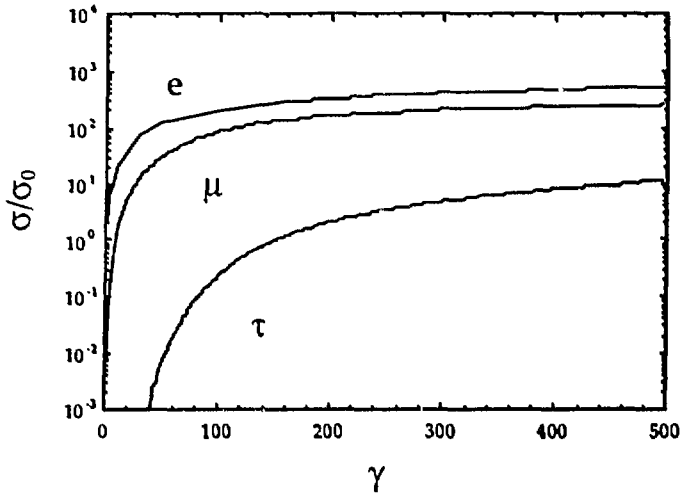

Fig. 8. Comparison of electromagnetic and Drell-Yan spectra for muon pairs.

the doubly differential cross sections (in rapidity and invariant mass) have a crossover point. As beam energy increases, electromagnetic pair production rises, whereas the Drell-Yan decreases.

The effects of the nuclear form factors on the heavy lepton production can be understood in greater depth by examining their effect on transverse momentum distributions, which is illustrated in Fig. 9, comparing electrons and muons. Again, we are considering colliding beams of Au nuclei at 100 GeV per nucleon and cross sections for singles. The effect of the form factor is seen below a momentum corresponding to the Compton wavelength of the muon; at

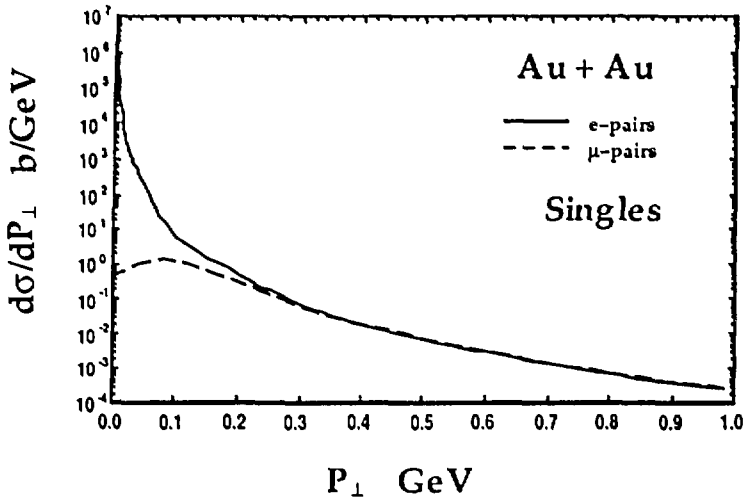

Fig. 9. Tranverse momentum spectra for electron and muon pairs.

higher momenta the spectrum is universal, as though for massless particles.

4. PRODUCTION OF W BOSONS

The principles underlying the foregoing calculations of lepton production can be extended to the coherent production of $W^{\pm}$ pairs and the Higgs boson. The lowest order Feynman diagrams contributing to W-pair production are shown in Fig. 10. The Feynman formulation guarantees gauge invariance, and we have found this to be useful as an algebraic and numeric check.

Using the above terms, the W-pair production cross-section is given by

$$\sigma_{ab\to W^-W^+} = \int \frac{d^3k_1 d^3k_2}{(2\pi)^6 2\omega_1 2\omega_2} \int d^2b \sum_{\lambda_1,\lambda_2} | < \vec{k}_1\lambda_1\vec{k}_2\lambda_2|S^{(1)} + S^{(2)}|0 > |^2 , \quad (16)$$

where $\vec{k}_1, \vec{k}_2$ are the momenta of the W^+, W^-, respectively, and where λ_1, λ_2 are their corresponding polarizations; $\vec{b}$ is the impact parameter. With a modest amount of analysis, the S-matrix in (16) can be cast into the form

$$< \vec{k}_1\lambda_1\vec{k}_2\lambda_2|S^{(1)} + S^{(2)}|0 > = -ie^2 \int \frac{d^4p}{(2\pi)^4} \; \epsilon^{\mu}_{\lambda_1}(k_1)\epsilon^{\nu}_{\lambda_2}(k_2)$$

$$\times \{g_{\mu\nu}A_\delta(-p+k_1)A^\delta(p+k_2) - A_\mu(-p+k_1)A_\nu(p+k_2)$$

$$+ B_{\mu\tau}(-p+k_1,p)\frac{f^{\tau\sigma}(p)}{p^2 - M_W^2}C_{\sigma\nu}(p+k_2,p)\}, \qquad (17)$$

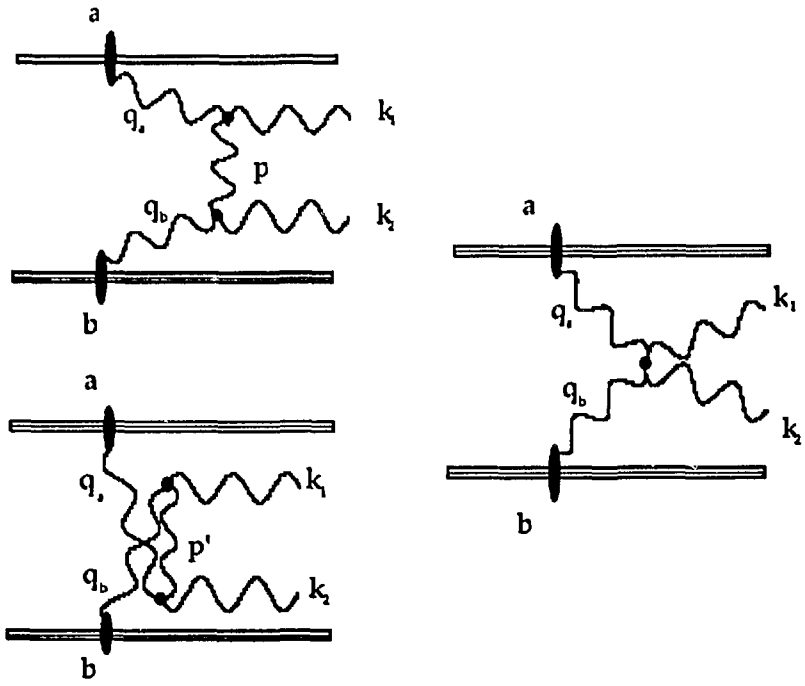

Fig. 10. Feynman diagrams for W pair production.

where we employ the conventions and normalization of Ref. [10] except that in the fermion normalization, we replace $2\sqrt{\vec{p}^2 + m^2}$ by $2|p_0|$. The functions $B_{\mu\nu}$, $C_{\mu\nu}$ and $f^{\mu\nu}$ are defined as

$$B_{\mu\nu}(q,p) = (q_\mu - p_\mu)A_\nu(q) - A_\mu(q)(q_\nu + k_{1\nu}) + g_{\mu\nu}(p_\delta + k_{1\delta})A^\delta(q);$$

$$C_{\mu\nu}(q,p) = (q_\mu + k_{2\mu})A_\nu(q) - A_\mu(q)(q_\nu + p_\nu) + g_{\mu\nu}(p_\delta - k_{2\delta})A^\delta(q);$$

$$f^{\mu\nu}(p) = -g^{\mu\nu} + p^\mu p^\nu / M_W^2. \qquad (18)$$

The integration over the impact parameter can be carried out analytically, leading to the cross section expression

$$\sigma_{ab\to W^-W^+} = \frac{Z_a^2 Z_b^2 (4\pi\alpha)^4}{4\beta^2} \int \frac{d^3k_1 d^3k_2 d^2p_\perp}{(2\pi)^8 2\omega_1 2\omega_2} f_a^2(q_a^2) f_b^2(q_b^2) \sum_{\lambda_1,\lambda_2} |\epsilon^\mu_{\lambda_1}(k_1)\epsilon^\nu_{\lambda_2}(k_2)$$
$$\times \{2g_{\mu\nu} u^a \cdot u^b - u^a_\mu u^b_\nu - u^b_\mu u^a_\nu + \hat{B}^a_{\mu\tau}(q_a,p) \frac{f^{\tau\sigma}(p)}{p^2 - M_W^2} \hat{C}^b_{\sigma\nu}(q_b,p)$$
$$+ \hat{B}^b_{\mu\tau}(q_b,p') \frac{f^{\tau\sigma}(p')}{p'^2 - M_W^2} \hat{C}^a_{\sigma\nu}(q_a,p')\}|^2 \,. \tag{19}$$

The four-momenta, (q_a, q_b) are carried by the fields of each nucleus, and (p, p') are the corresponding momenta of the intermediate boson line in the direct and crossed diagram respectively. Four-momentum conservation at the vertices in Fig. 10 reduces the number of integrations, and relates the photon momenta to those of the particles in the final state. For pair production of massive charged particles, both of the virtual photons q_a,q_b are considerably "off-shell". The functions with "hats" appearing in the cross section expression (19), are obtained from (18) upon replacing the fields A_μ by the corresponding vectors $u^{a,b}_\mu$:

$$\hat{B}^{a,b}_{\mu\nu}(q,p) = (q_\mu - p_\mu) u^{a,b}_\nu - u^{a,b}_\mu (q_\nu + k_{1\nu}) + g_{\mu\nu}(p^\delta + k_1^\delta) u^{a,b}_\delta$$
$$\hat{C}^{a,b}_{\mu\nu}(q,p) = (q_\mu + k_{2\mu}) u^{a,b}_\nu - u^{a,b}_\mu (q_\nu + p_\nu) + g_{\mu\nu}(p^\delta - k_2^\delta) u^{a,b}_\delta \,. \tag{20}$$

The total cross section for W production as a function of energy is shown in Fig. 11. Assuming as a rule of thumb that the largest heavy ion colliders have a luminosity of one pb^{-1} per accelerator year of 10^7 seconds, we arrive at annual yields of 10^3 at LHC and 10^5 at SSC. These are usable rates, though falling short of factory levels of production.

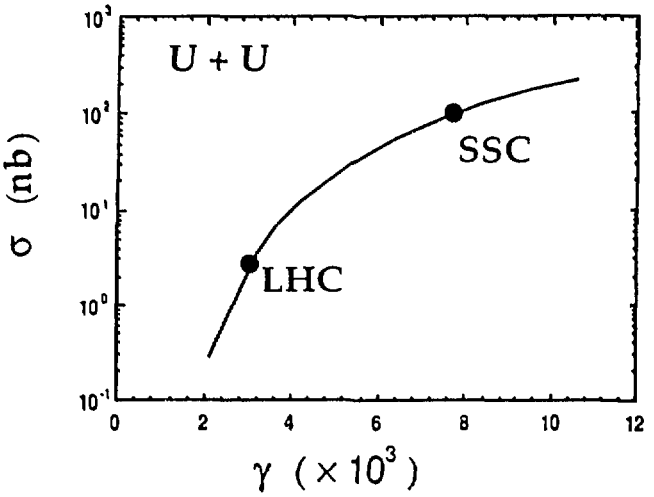

Fig. 11. Total W pair production *vs* energy.

5. PRODUCTION OF THE HIGGS

Since the Higgs boson is a neutral particle it does not directly couple to electromagnetic fields. The coherent production of the Higgs via two-photon processes can occur through the generation and subsequent fusion of charged pairs. The lowest-order Feynman diagram for this process is shown in Fig. 12, in which the intermediate loops can be formed from any quarks or leptons, or charged bosons. The contribution of these loops is usually treated as an effective three-body vertex or interaction Hamiltonian [11] of the form

$$\mathcal{H}_{\rm int} = \frac{e^2}{2} I : F^{\mu\nu} F_{\mu\nu} H : , \tag{21}$$

where

$$I = \frac{g}{8\pi^2 M_W} (A_q + A_\ell + A_W) , \tag{22}$$

and where each amplitude A_i depends on the ratio of masses, $\lambda_i = m_i^2/M_H^2$ through complicated expressions which can be found in the literature [11]. The squared coupling strength for the Lagrangian is shown in Fig. 12 as a function of the

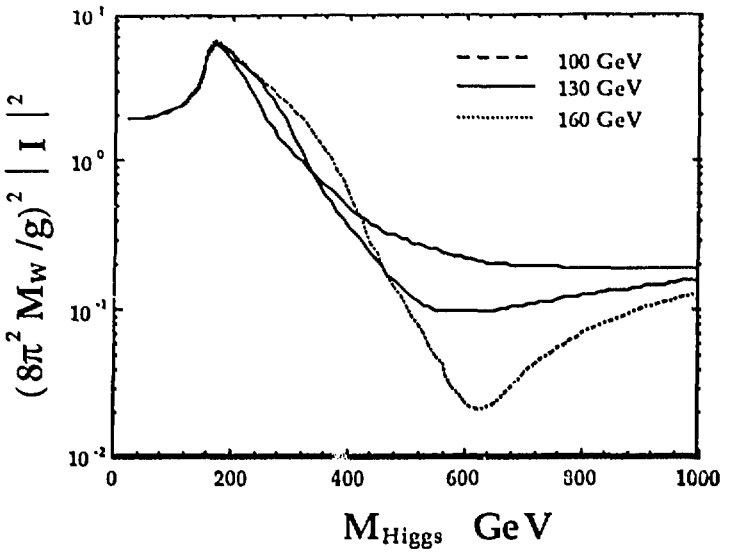

Fig. 12. Coupling strength entering the effective Lagrangean for Higgs production.

Higgs mass. Results are presented for three different values of the top quark mass, 100, 130, and 160 GeV, within the limits determined in Ref. [12]. There is a considerable variation in the coupling for the three values for the range of Higgs masses shown. For an intermediate mass Higgs less than about 250 GeV, the coupling parameter is not sensitive to the top quark mass, and we make the choice $m_t = 100$ GeV. The Higgs production cross section is obtained from the S-matrix term which is first order in the Hamiltonian (21)

$$\sigma_{ab\to H_0} = \int d^2b \int \frac{d^3k}{(2\pi)^3 2\omega_k} \left| < \vec{k}|S^{(1)}|0 > \right|^2 , \tag{23}$$

where

$$< \vec{k}|S^{(1)}|0 > = ie^2 I \int \frac{d^4q_1 d^4q_2}{(2\pi)^4} \delta^{(4)}(q_1 + q_2 - k)$$
$$\times [(q_1 \cdot q_2) A_\mu(q_1) A^\mu(q_2) - q_{1\mu} A^\mu(q_2) q_{2\nu} A^\nu(q_1)]. \qquad (24)$$

After carrying out the integral over the impact parameter, we have the resulting total cross section expression

$$\sigma_{ab \to H_0} = \frac{4 Z_a^2 Z_b^2 (4\pi\alpha)^4 |I|^2}{\beta^2} \int \frac{d^3k d^2q_{a\perp} d^2q_{b\perp}}{(2\pi)^5 2\omega_k} \delta^{(2)}(\vec{q}_{a\perp} + \vec{q}_{b\perp} - \vec{k}_\perp) f^2(q_a^2) f^2(q_b^2)$$
$$\times \left[(q_a \cdot q_b)(e^a \cdot e^b) - (q_a \cdot u^b)(q_b \cdot u^a)\right]^2 . \qquad (25)$$

For a Higgs boson with a mass of about 100 GeV and a top quark mass above 100 GeV, the lifetime of the Higgs is governed mainly by its decay into b-quark pairs evolving into jets. The calculated decay width yields a lifetime of about 10^{-25}s, so that the production and decay of the Higgs occurs promptly and does not depend on the subsequent evolution of the nuclear collision. The total cross sections, given in Fig. 13 as a function of energy, are experimentally realizable.

However, for central heavy-ion collisions, the nuclei will undergo very strong excitations which remove them from the elastic flux and hence reduce the cross section. In a semiclassical model [13], the probability for making the Higgs is a function of the impact parameter as described in (23). Along a definite impact parameter b, we introduce a transmission function $s(b)$, which is the probability that the nuclei will remain in their ground state during the collision. Modifying (25) accordingly results in the following expression for the Higgs production,

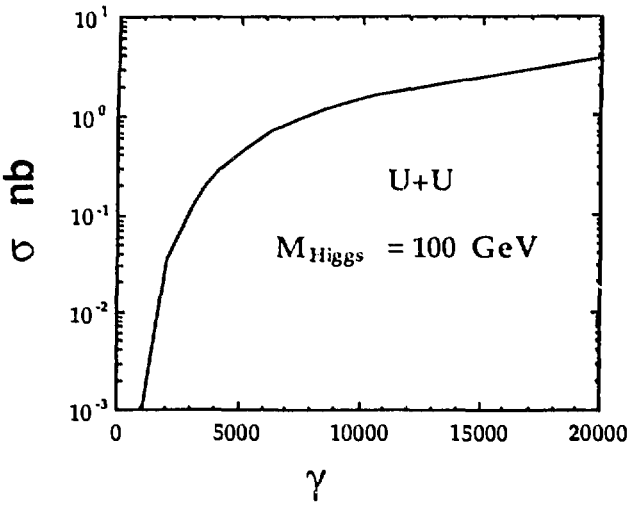

Fig. 13. Total Higgs production vs energy.

$$\sigma_{ab\to H_0} = \int d^2b\, s(b) \int \frac{d^3k}{(2\pi)^3 2\omega} | < \vec{k}|S^{(1)}|0 > |^2 . \tag{26}$$

This equation provides a simple estimate of the reduction in the cross section due to nonelastic final channels of nuclei.

The impact parameter dependence of the S-matrix elements for the two-photon process can be written explicitly as

$$< f|S|0 >= \int \frac{d^2q_\perp}{(2\pi)^2} M_f(\vec{q}_\perp) \exp\{i(\vec{q}_\perp - \vec{k}_{f\perp}/2)\cdot\vec{b}\}, \tag{27}$$

where M_f is independent of b. The total cross section thus reduces to the following form

$$\sigma_{ab\to f} = \sum_f \int \frac{d^2q_{1\perp}}{(2\pi)^2} \frac{d^2q_{1\perp}}{(2\pi)^2} M_f(\vec{q}_{1\perp}) M_f^*(\vec{q}_{2\perp}) S(\vec{q}_{1\perp} - \vec{q}_{2\perp}), \tag{28}$$

where $S(\vec{q}_\perp) = \int d^2b\, s(b) \exp(i\vec{q}_\perp \cdot \vec{b})$.

We use a Fermi function for $s(b)$, though the results are not greatly different for other models. In Fig. 14 we plot the cross section for Higgs production, $\sigma(0) - \sigma(R_0)$, as a function of the cutoff parameter R_0 for collisions of uranium at a beam energy of 3.5 TeV per nucleon.

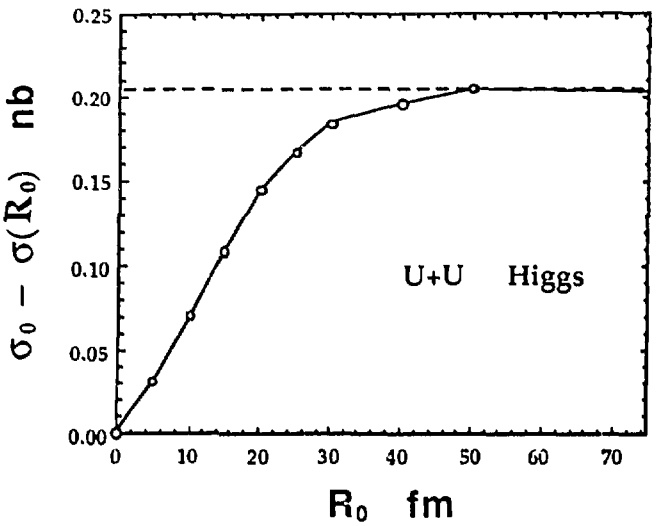

Fig. 14. Dependence of the Higgs cross section on the absorption cutoff distance.

The calculation of the impact parameter dependence entails an additional convolution integral over an oscillating Bessel function, and we need about 50 times more Monte Carlo points to reach the same precision as before. As $R_0 \to \infty$, $\sigma(R_0) \to 0$, and the cross section converges to the previous results, as shown by the dashed line.

These figures show that a significant part of the cross section comes from impact parameters between two and four times the nuclear radius (about 8 fm), and very little comes from larger impact parameters. At $R_0 = 30$ fm the cross section has been depleted by about a factor of ten. Even for these separations, Coulomb

excitation of the nuclei can lead to strong inelastic excitation. The argument made in Sect. 2.2 demonstrates that at higher beam energies, a greater fraction of the coherent production is shifted to the peripheral impact parameter region. Exclusion of the central events at $2R$, where R is the nuclear radius, reduces the cross section of Higgs production by a factor of 1.9 at LHC (3.5 TeV), by a factor of 1.4 at SSC (8TeV), and by a factor of 1.2 at ELOISATRON (40TeV).

Having established that backgrounds from hard hadronic processes in central collisions can be eliminated, we still must contend with the intrinsic backgrounds due to peripheral electromagnetic production of possible decay products. The formalism outlined above can be extended to predict the spectra of Higgs decay products, notably b-jets. Fig. 15 shows the singles spectrum of b-quarks, as a function of transverse momentum following a Higgs decay. The characteristic kinematic peak appears at half the Higgs mass. However the peak is somewhat below the background, and probably unobservable. All singles spectra exhibit the same characteristic drawback. A simple scheme for eliminating backgrounds entirely is available, though it involves a more sophisticated jet analysis. It is simply required to detect pseudo-pairs of electrons or muons, e.g. from $H \rightarrow W^+W^-$ decay chains, but rejecting pairs with *combined* transverse momenta of less than a few times 0.1 GeV. This will remove all background "true" pairs, which are produced at almost zero transverse pair momentum, while leaving the pseudo-pairs, whose momenta extend to hundreds of GeV.

Finally, we have examined the rate of production of the Higgs by incoherent

processes, essentially parton collisions. The formalism developed earlier is readily extended to inelastic processes, and requires as additional knowledge, the inelastic

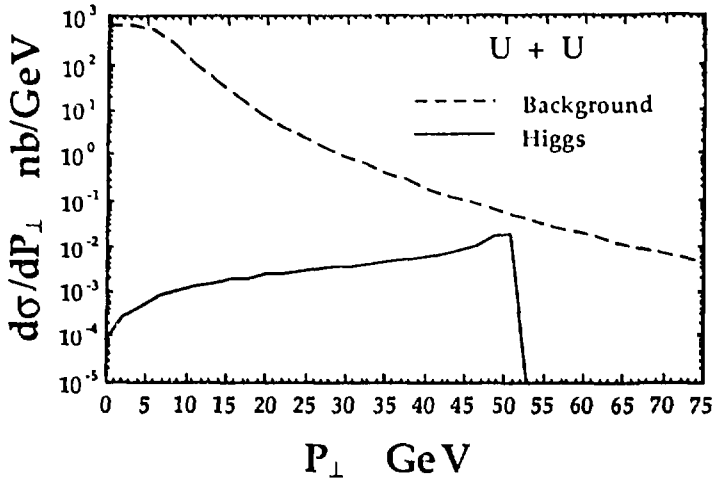

Fig. 15. Spectrum of b-pairs (singles transverse momentum) from Higgs decay compared with the background of direct electromagnetic production.

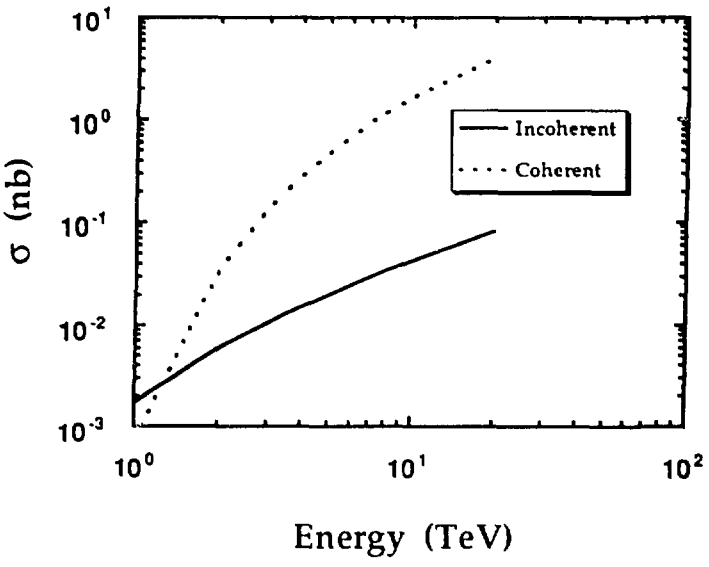

Fig. 16. Incoherent Higgs production in U+U collisions.

structure functions for electron-nucleus scattering [14]. Using fits to measured structure functions, we calculate the cross section shown in Fig. 16, with the coherent result for comparison. The incoherent is much smaller above one TeV. It is interesting to examine the contributions from different régimes of q^2 and Feynman x. Large inelasticities (small x) dominate, as shown in Fig. 17.

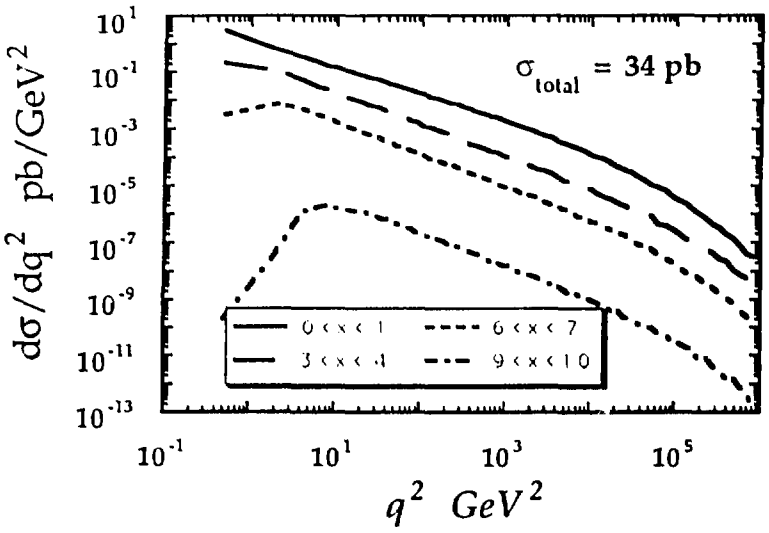

Fig. 17. Incoherent Higgs production in U+ U collisions: cross sections differential in momentum tranfer for different cuts on Feynman x.

6. CONCLUSIONS

We conclude that electromagnetic production provides a clean method of detecting a Higgs, even of intermediate mass, say 0.5 TeV. The yields are not much less than those for conventional p-p schemes, but advantages lie in the conceptual simplicity of the underlying theory, and for experimentalists, the possibility of eliminating most backgrounds without elaborate data analysis. The estimates

we have arrived at for LHC and SSC energies suggest that the feasibility of injecting heavy ions in the SSC deserves at least a pilot study. In the realm of linear colliders, the possibility exists of using coherence among the charged particles in a bunch to enhance production rates. Such studies are underway.

7. ACKNOWLEDGEMENTS

This research was sponsored by the U.S. D.O.E. under contract DE-AC05-84OR21400 managed by Martin Marietta Energy Systems Inc.

REFERENCES

1. J.D. Bjorken and L. McLerran, Phys. Rev. **D31**, 63 (1985).

2. C. Bottcher and M.R. Strayer, in "Physics of Strong Fields", ed. W. Greiner, (Plenum, New York, 1987), Vol. **153**, p. 629.

3. C. Bottcher and M.R. Strayer, Phys. Rev. **D39**, 1330 (1989); Nucl. Inst. and Meth. **B31**, 122 (1988); Nucl. Inst. and Meth. **B40**, 354 (1989); J.S. Wu, C. Bottcher and M.R. Strayer, Phys. Rev. **C43** , 2422 (1991).

4. G. Baur and C.A. Bertulani, Phys. Rep. **161**, 299 (1988); J. Rau, B. Müller, W. Greiner and G. Soff, J. Phys. **G15**, L25 (1989); G. Racah, Nuovo Cimento, **14**, 70 (1937).

5. Elena Papageorgiu, Phys. Rev. **D40** , 92 (1989); Nucl. Phys. **A498**, 593c (1989); M. Drees, J. Ellis and D. Zeppenfeld, Phys. Lett. **B223**, 454 (1989); M. Grabiak,

B. Müller, W. Greiner, G. Soff, and P. Koch, J. Phys. **G15**, L25 (1989).

6. J.S. Wu, C. Bottcher, M. R. Strayer, A.K. Kerman, to appear in Ann. Phys. (N.Y.), 1991.

7. R.N. Cahn and J.D. Jackson, Phys. Rev. **D40**, 3690, (1990); B. Müller and A.J. Schramm, Phys. Rev. **D40**, 3696, (1990); J.S. Wu, C. Bottcher, M. R. Strayer and A.K. Kerman, Particle World, **1**, 174 (1990).

8. C. Bottcher and M.R. Strayer, in "Proc. of the Summer School of Computational Atomic and Nuclear Physics", p 118, (World Scientific, Teaneck, NJ, 1990).

9. G.R. Satchler, *Introduction to Nuclear Reactions*, (Macmillan, London, 1990).

10. J. D. Bjorken and S. D. Drell, *Relativistic Quantum Mechanics*, (McGraw-Hill, New York, 1964).

11. J. Ellis, M.K. Gaillard and D.V. Nanopoulos, Nucl. Phys. **B106**, 292 (1976); Vernon Barger and Roger Phillips, *Collider Physics*, (Addison-Wesley, New York, 1987).

12. J. Ellis and G.L. Fogli, CERN preprint, CERN-TH.5511/89, August 1989.

13. C. Bottcher and M.R. Strayer, J. Phys. **G16**, 975 (1990).

14. J.S. Wu, C.M. Shakin, C. Bottcher and M.R. Strayer, Phys. Rev. **C43** , 2422 (1991).